Journal of Sound and Vibration (1998) **209**(1), 163–186

LOW DIMENSIONAL MODELS OF SHELL VIBRATIONS. PARAMETRICALLY EXCITED VIBRATIONS OF CYLINDRICAL SHELLS

A. A. Popov and J. M. T. Thompson

Centre for Nonlinear Dynamics and its Applications, University College London, Gower Street, London WC1E 6BT, England

and

F. A. McRobie

Engineering Department, University of Cambridge, Trumpington Street, Cambridge CB2 1PZ, England

(*Received* 7 *May* 1997, *and in final form* 18 *September* 1997)

Vibrations of cylindrical shells parametrically excited by axial forcing are considered. The governing system of two coupled non-linear partial differential equations is discretized by using Lagrange equations. The computation is simplified significantly by the application of computer algebra and as a result low dimensional models of shell vibrations are readily obtained. After applying numerical continuation techniques and ideas from dynamical systems theory, complete bifurcation diagrams are constructed. The principal aim is to investigate the interaction between different modes of shell vibration. Results for system models with two of the lowest modes are discussed.

1. INTRODUCTION

The thin cylinder under axial load is a fundamental problem in shell theory mainly due to its wide use as a structural element in several engineering areas: civil, mechanical, aeronautical, and nuclear. The complete circular cylindrical shell combines a simple geometric shape with an extremely complex behaviour under external loading. Cylindrical shells have been the subject of a great number of studies, mainly within the context of elastic buckling under static loading; see e.g. references [1–5]. At the same time the behaviour of cylindrical shells under dynamic loading is much less understood [6, 7]. An important problem in structural dynamics concerns parametrically excited shell vibrations. They have been treated mostly by classical linear methods from dynamic stability theory [8–10]. Such stability analyses provide only an outline of the parameter regimes where non-linear effects are of significance. They cannot reveal important details about the bifurcations and detect only the loss of stability of the trivial solution without giving answers about the possible outcomes of the bifurcation. The analysis of more complicated motions is usually limited to a simple numerical integration [11, 12].

An important phenomenon connected with shell dynamics is the possible coupling or interaction between different modes [13, 14]. It is well known that there is a basic difference in the frequency spectrum of a cylinder as compared to those of strings, membranes, beams, and plates [15]. The frequency spectrum of a cylinder rarely follows any simple rule. Often several successive frequencies are very closely grouped together. The high modal

0022–460X/98/010163 + 24 $25.00/0/sv971279

densities in shells facilitate the modal interactions. Results on modal interaction in shells have been reported in reference [16], where the main problems are stated and the analytical analysis is performed together with some experiments. Zones of dynamic instability are identified by the reduction to equations of Mathieu type and the successive application of perturbation methods. Although the perturbation analysis delineates modal interactions, this is clearly only the first step towards the understanding of the full picture.

The aim of the present study is to investigate as completely as possible bifurcations and stability of solutions of low dimensional models of parametrically excited cylindrical shells. The main concern is the modal interactions and their relevance to the behaviour of the structure under consideration. The mathematical modelling is based on the equations of the shallow shell theory, namely the Donnell equations. This formulation is selected on the basis that it is the simplest approach which retains the essential non-linear features of the problem. We have been very careful in our choice of appropriate approximation functions in order to capture the essential dynamics. The system equations are discretized by the use of Lagrange equations and all analytical manipulations are performed through symbolic computations. The main tool of our study of bifurcations and stability of solutions is numerical continuation techniques.

2. MECHANICAL SYSTEM

The structure considered is an infinitely long circular cylindrical shell subjected to a uniformly distributed periodic forcing acting in the surface of the shell, namely the parametric excitation; see Figure 1. Within the infinitely long shell, we focus on deformations that are axially periodic with wavelength L. The points at the periodic boundaries are allowed to pulsate radially, in a way that the local cross-section always remains circular and concentric with its original configuration. By considering an infinitely long cylinder we concentrate on the modal interactions and avoid the well-known problems that arise by satisfying the boundary conditions at both ends of the cylinder. We are aware that the complete satisfaction of the boundary conditions is a difficult mathematical task and may also be of importance for some applications. We refer the reader to reference [17] for an extensive discussion on that issue. The shell is made of homogeneous material such as steel or aluminium. We take into consideration dissipation of energy both in the environment and in the shell, namely linear viscous damping from the surrounding air, plus viscoelastic material damping, respectively.

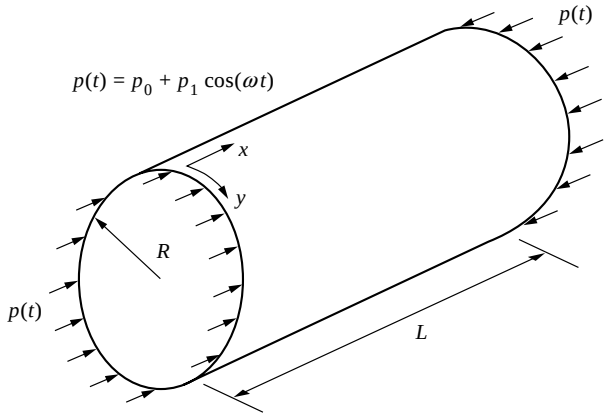

Figure 1. Cylindrical shell under parametric excitation.

All physical parameters except the loading are usually fixed, and we thus investigate the phenomena observed when the forcing is varied. For moderate static load and small dynamic amplitude the shell vibrates in a radially symmetric mode. This is predominantly axial with some dilation due to Poisson's ratio effects. For the small vibrations covered by Donnell's equations, the bending associated with such dilation (due to the change of curvature) is assumed negligible. On increasing the dynamic forcing amplitude such cylindrical motions can lose stability: lateral-flexural motions arise which are out-of-cylinder sinusoidal oscillations, both in the axial and circumferential directions. This is the so-called parametric resonance: one puts energy directly into the axial mode but obtains motions involving modes orthogonal to the excitation.

A completely new behaviour occurs under a further increase of the static component of the loading. The shell can snap through to a large amplitude, stable equilibrium where the shell has buckled into a checkerboard pattern of lateral deflections, and vibrations in the vicinity of this new deformed state can occur. This static snap-through buckling phenomena has been studied extensively [1–3].

3. MATHEMATICAL MODEL

Non-linear vibrations of a thin cylindrical shell are described by a system of two coupled partial differential equations of the form

$$m\frac{\partial^2 w}{\partial t^2} + \beta_1\frac{\partial w}{\partial t} + \beta_2\frac{\partial}{\partial t}\Delta^2 w + D\Delta^2 w = \frac{1}{R}\frac{\partial^2 \Phi}{\partial x^2} + [\Phi, w], \tag{1}$$

$$\frac{1}{Eh}\Delta^2\Phi = -\frac{1}{R}\frac{\partial^2 w}{\partial x^2} - \tfrac{1}{2}[w, w], \tag{2}$$

where

$$[f, g] = \frac{\partial^2 f}{\partial x^2}\frac{\partial^2 g}{\partial y^2} - 2\frac{\partial^2 f}{\partial x\,\partial y}\frac{\partial^2 g}{\partial x\,\partial y} + \frac{\partial^2 f}{\partial y^2}\frac{\partial^2 g}{\partial x^2}.$$

In equations (1) and (2) and Figure 1, x is the meridional length co-ordinate, y the circumferential length co-ordinate, t time, R radius of the cylinder, h shell thickness, w normal displacement (positive inwards), Φ in-plane stress (Airy) function and Δ^2 is the biharmonic operator. The material is elastic, isotropic and the mid-surface is used as a reference surface. Thus, E is the Young's modulus, ν the Poisson's ratio, m mass per unit area, β_1 and β_2 damping coefficients, and $D = Eh^3/12(1-\nu^2)$ is the bending stiffness of the shell.

The periodic excitation has the form

$$p(t) = p_0 + p_1\cos(\omega t)$$

where p_0 is the static load, p_1 the amplitude of the dynamic part of the load and ω is the frequency of excitation.

The governing PDEs are of quasi-linear hyperbolic type. This system was introduced by von Kármán in 1910 for plates: i.e., without the terms depending on the radius R. Subsequently in 1933 Donnell suggested equations (1) and (2) for shallow shell problems.

The main assumptions in the derivation of equations (1) and (2) are as follows: in-plane inertia is neglected and consequently only transversal bending motions are considered; the non-linearities in curvature strains are ignored, but the non-linearities in the mid-plane stretching strain terms are retained in the strain-displacement relations; Donnell's approximation $a/R \leqslant \pi/5$, where a is the circumferential half wavelength, is assumed to

hold; and $h \ll R$ (the usual thin shell assumption) and transverse shear and rotatory inertia efforts are neglected.

4. FINITE DIMENSIONAL MODELS

The usual approach when dealing with infinite dimensional systems represented by PDEs is to reduce them to approximate finite dimensional systems. There are several well-known methods for performing this task: the Rayleigh–Ritz method, Galerkin approximations, finite differences, finite and boundary element methods, and recently inertial manifolds. One approximates the motion with a finite number of degrees of freedom in the hope that the essential dynamics is captured.

Here we obtain finite dimensional models by using Lagrange equations with appropriate approximation functions for the lateral displacement. At this stage the main difficulties are the choice of the approximation (ansatz) functions, and the calculation in the Lagrange equations requires a significant amount of analytical manipulations. We can satisfactorily solve the second problem by using general computer algebra routines. The main advantage of their use is that the system is treated relatively easily with as many d.o.f. as required. We will describe briefly the corresponding procedure. The deflection w is represented notionally in the form [17]

$$w(x, y, t) = \sum_{k=0}^{\infty} \sum_{n=0}^{\infty} q_{kn}(t) h \cos\left(\frac{k\pi x}{L}\right) \cos\left(\frac{ny}{R}\right). \tag{3}$$

Usually, one takes only the first few terms in equation (3). For dynamical problems vibration modes with different numbers of waves both axially and circumferentially must be included in the analysis, when their frequencies are related through resonance conditions between them and the frequency of the loading. We will illustrate this point with the results. The frequency of excitation is the major factor that determines which modes come into play.

For a general discussion on the choice of the form for w within the context of elastic buckling, see reference [18]. Briefly, the motivation is based on the post-buckling behaviour of the shell and is as follows. Large transversal deflections of the cylinder carry an underlying asymmetry, inwards being fundamentally different from outwards. Each of the modes taken into consideration is symmetric in its own right, being harmonic axially and circumferentially. It is only by combining that the modes can satisfy the required asymmetry, and this makes mode interaction inevitable. There is a principal difference between the mode interaction in the static and dynamic case, in the sense that completely different modes can interact with each other in both cases.

Our system is as idealized as possible, being an infinitely long, thin cylindrical shell, with periodic boundary conditions, imperfection free, restrained against overall buckling as a column. Our main interest focuses on the interaction between the separate modes taken into consideration.

The total potential energy manifests important properties of the system under investigation. In some cases it is even more suitable for the analysis than the governing partial differential equations. By making use of potential energy expressions in Lagrange equations we will derive systems of ordinary differential equations which govern the dynamics of the cylindrical shell. This approach is also widely used for other problems such as bars, rods, beams, and plates, and it is known as the Rayleigh–Ritz method.

The Lagrange equation for any generalized co-ordinate of a general mechanical system is

$$\frac{\mathrm{d}}{\mathrm{d}t}\left(\frac{\partial L}{\partial \dot{q}_i}\right) - \frac{\partial L}{\partial q_i} = Q_i, \qquad i = 1, 2, \ldots, \tag{4}$$

where q_i is the generalized co-ordinate, and the Lagrangian function $L \equiv T - V$, where T is the kinetic energy and V the potential energy of the system. The Q_i are those generalized forces not derivable from a potential function. In our case these are friction forces and time-variant forcing functions. It is important to note that all load-dependent terms will be considered through the generalized forces Q_i, and not through the potential energy function V as is the usual case when studying elastic buckling.

We will introduce briefly the relevant energy expressions; for more details see references [4, 5]. The total potential energy in our case is the strain energy of the cylindrical shell. The strain energy consists of stretching or extensional elastic energy U_s and bending energy U_b. The stretching elastic energy can be written as

$$U_s = \frac{1}{2Eh}\int_0^L \int_0^{2\pi R} \{(\Delta\Phi)^2 - (1+\nu)[\Phi, \Phi]\}\,\mathrm{d}x\,\mathrm{d}y \tag{5}$$

while the bending energy is

$$U_b = \frac{D}{2}\int_0^L \int_0^{2\pi R} \{(\Delta w)^2 - (1-\nu)[w, w]\}\,\mathrm{d}x\,\mathrm{d}y. \tag{6}$$

In both expressions the integration is over the surface area of the shell and Δ stands for the Laplace operator. A simplified form of equations (5) and (6) is obtained after integrating by parts and by employing the fact that only periodic variations in x and y of w are considered:

$$U_s = \frac{1}{2Eh}\int_0^L \int_0^{2\pi R} (\Delta\Phi)^2\,\mathrm{d}x\,\mathrm{d}y, \qquad U_b = \frac{D}{2}\int_0^L \int_0^{2\pi R} (\Delta w)^2\,\mathrm{d}x\,\mathrm{d}y. \tag{7, 8}$$

Finally the total potential energy of the shell is obtained as

$$V = U_s + U_b. \tag{9}$$

The kinetic energy is written as

$$T = \tfrac{1}{2}\int_0^L \int_0^{2\pi R} m\left(\frac{\partial w}{\partial t}\right)^2 \mathrm{d}x\,\mathrm{d}y. \tag{10}$$

In order to calculate the generalized forces Q_i one needs expressions for the virtual work done by the applied axial loading and friction forces. The virtual work done by the external forces is written as

$$W_p = -\frac{p(t)}{2}\int_0^L \int_0^{2\pi R} \left\{\frac{\partial^2 \Phi}{\partial y^2} - \nu\frac{\partial^2 \Phi}{\partial x^2} - \left(\frac{\partial w}{\partial x}\right)^2\right\}\mathrm{d}x\,\mathrm{d}y. \tag{11}$$

A similar reduction as for the potential energy function may be used, to give

$$W_p = \frac{p(t)}{2} \int_0^L \int_0^{2\pi R} \left(\frac{\partial w}{\partial x}\right)^2 \mathrm{d}x\, \mathrm{d}y. \tag{12}$$

The usual approach when dealing with friction forces in the context of the Lagrange equations is to calculate the Rayleigh dissipation function [19] which in our case is

$$R_e = \tfrac{1}{2}\beta_1 \int_0^L \int_0^{2\pi R} \left(\frac{\partial w}{\partial t}\right)^2 \mathrm{d}x\, \mathrm{d}y + \tfrac{1}{2}\beta_2 \int_0^L \int_0^{2\pi R} \left(\Delta \frac{\partial w}{\partial t}\right)^2 \mathrm{d}x\, \mathrm{d}y. \tag{13}$$

The first term stands for linear viscous forces due to air resistance while the second one is for viscoelastic material forces, respectively.

The generalized forces are obtained by a simple differentiation of the above functions

$$Q_i = -\partial R_e/\partial \dot{q}_i + \partial W_p/\partial q_i. \tag{14}$$

Now after approximating the system by a finite number of degrees of freedom it is possible to define Lagrange equations. Apart from w the stress function Φ is needed. Substituting equation (3) into the right side of equation (2) one may solve for Φ as a particular solution Φ_{par} which is completely determined by equation (2). With Φ expressed in terms of $q_i(t)$ $(i = 0, 1, 2, \ldots)$, one obtains Lagrange equation by the use of equations (7), (8), (10), (12) and (13). We can satisfactorily perform all calculations involved by using general computer algebra routines.

A note on the calculation of the stress function Φ is necessary. We have taken only the particular solution of Φ because in our case the homogeneous solution is equal to zero. One usually takes into accout the contribution of the static axial loading with the homogeneous solution. However, in the Lagrangian formulation it seems to us more appropriate to consider the contribution of the periodic axial loading through the generalized forces in the expression for virtual work W_p. Nevertheless, the most important problem with respect to the so-obtained function Φ from the physical point of view, is that the assumed form for w effectively defines stresses different from zero and periodic in y at $x = 0, L$. The peculiarity is that their contribution is negligible on the average (integrally). As we previously mentioned, we consider an infinitely long cylinder in order to avoid all problems connected with the exact (pointwise) satisfaction of the boundary conditions in stresses.

Let us take now for the approximation function the following expression [11]:

$$\begin{aligned} w(x, y, t) = {} & q_0(t)h + q_1(t)h \cos(\pi x/L) \cos(ny/R) \\ & + q_2(t)h \cos(2\pi x/L) + q_3(t)h \cos(2ny/R). \end{aligned} \tag{15}$$

Here the q_0-term takes into account the radial displacements of the points at the boundaries. The second term corresponds to small amplitude bending deflections according to the linear buckling and vibration theory. The last two terms are of significance when dealing with large displacements and generate asymmetric structural response in the direction of the inwards and outwards normal to the cylinder. The above chosen combination of modes is capable of describing the well-known Yoshimura or diamond pattern.

After using our symbolic algebra code we obtain, for the potential function,

$$\begin{aligned} V = {} & \tfrac{1}{2}V^0_{11}q_1^2 + \tfrac{1}{2}V^0_{22}q_2^2 + \tfrac{1}{2}V^0_{33}q_3^2 + \tfrac{1}{2}V^0_{112}q_1^2q_2 + \tfrac{1}{2}V^0_{113}q_1^2q_3 \\ & + \tfrac{1}{24}V^0_{1111}q_1^4 + \tfrac{1}{4}V^0_{1122}q_1^2q_2^2 + \tfrac{1}{4}V^0_{1133}q_1^2q_3^2 + \tfrac{1}{4}V^0_{2233}q_2^2q_3^2 + \tfrac{1}{2}V^0_{1123}q_1^2q_2q_3. \end{aligned} \tag{16}$$

This expression for the potential function is exact but is written in the form of a Taylor expansion about the unloaded equilibrium state, represented by superscript 0, the coefficients being given by

$$\frac{V_{11}^0}{V_c} = \frac{8\alpha^2}{\pi^2(1+\gamma^2)^2} + \frac{2\pi^2\beta^4(1+\gamma^2)^2}{3(1-\nu^2)}, \qquad \frac{V_{22}^0}{V_c} = \frac{16\alpha^2}{\pi^2} + \frac{64\pi^2\beta^4}{3(1-\nu^2)},$$

$$\frac{V_{33}^0}{V_c} = \frac{64\pi^2\beta^4\gamma^4}{3(1-\nu^2)}, \qquad \frac{V_{112}^0}{V_c} = -\frac{32\alpha\beta^2\gamma^2}{(1+\gamma^2)^2} - 4\alpha\beta^2\gamma^2,$$

$$\frac{V_{113}^0}{V_c} = -\frac{32\alpha\beta^2\gamma^2}{(1+\gamma^2)^2}, \qquad \frac{V_{1111}^0}{V_c} = 3\pi^2\beta^4(1+\gamma^4),$$

$$\frac{V_{1122}^0}{V_c} = 64\pi^2\beta^4\gamma^4\left(\frac{1}{(1+\gamma^2)^2} + \frac{1}{(9+\gamma^2)^2}\right), \qquad \frac{V_{2233}^0}{V_c} = \frac{256\pi^2\beta^4\gamma^4}{(1+\gamma^2)^2},$$

$$\frac{V_{1133}^0}{V_c} = 64\pi^2\beta^4\gamma^4\left(\frac{1}{(1+\gamma^2)^2} + \frac{1}{(1+9\gamma^2)^2}\right), \qquad \frac{V_{1123}^0}{V_c} = \frac{64\pi^2\beta^4\gamma^4}{(1+\gamma^2)^2}.$$

Here for simplicity of notations we have factored out a common multiplier:

$$V_c = \pi^3 EhRL/16.$$

The following non-dimensional parameters have been introduced in the above expressions:

$$\alpha = h/R, \qquad \beta = h/L, \qquad \gamma = Ln/\pi R.$$

Here the wavelength parameter γ is defined as the ratio of the axial to the circumferential wavelength of the q_1-mode. The expression (16) for the potential energy is given in reference [18] in slightly different notations.

The kinetic energy is

$$T = \tfrac{1}{2}T_{00}\dot{q}_0^2 + \tfrac{1}{2}T_{11}\dot{q}_1^2 + \tfrac{1}{2}T_{22}\dot{q}_2^2 + \tfrac{1}{2}T_{33}\dot{q}_3^2, \tag{17}$$

where the coefficients are

$$T_{00} = 2\pi mh^2RL, \qquad T_{11} = \tfrac{1}{2}\pi mh^2RL, \qquad T_{22} = \pi mh^2RL, \qquad T_{33} = \pi mh^2RL.$$

Similar computations give for the Rayleigh dissipation function

$$R_e = \tfrac{1}{2}R_{00}\dot{q}_0^2 + \tfrac{1}{2}R_{11}\dot{q}_1^2 + \tfrac{1}{2}R_{22}\dot{q}_2^2 + \tfrac{1}{2}R_{33}\dot{q}_3^2, \tag{18}$$

where

$$R_{00} = 2\pi\beta_1 h^2RL, \qquad R_{11} = \tfrac{1}{2}\pi\beta_1 h^2RL + \tfrac{1}{2}\pi^5\beta_2(\beta^3/\alpha)(1+\gamma^2)^2,$$

$$R_{22} = \pi\beta_1 h^2RL + 16\pi^5\beta_2(\beta^3/\alpha), \qquad R_{33} = \pi\beta_1 h^2RL + 16\pi^5\beta_2(\beta^3\gamma^4/\alpha),$$

and for the virtual work done by external forces

$$W_p = \tfrac{1}{2}W_{11}q_1^2 + \tfrac{1}{2}W_{22}q_2^2, \tag{19}$$

where

$$8W_{11} = W_{22} = 4p(t)(\pi^3h^2R/L).$$

5. DISCUSSION OF PROPERTIES FOR THE DISCRETE MODELS

It seems reasonable to analyze some properties of the discrete models obtained for a better understanding of the shell vibrations. If we look at the expressions for the potential

energy (16), the kinetic energy (17), the Rayleigh dissipation function (18) and the virtual work (19), and take only the quadratic terms in equation (16), it is evident that all these forms are simultaneously diagonalized through the choice of the approximation function (15). The different terms in equation (15) are normal modes of vibration for the linearized system. It is easy now to obtain quantities with important physical meaning for the problem investigated, namely frequencies of linear vibration, critical loads, damping ratios, etc.

The small-amplitude linear vibrations are governed by the system

$$T_{ii}\ddot{q}_i + R_{ii}\dot{q}_i + V^0_{ii}q_i = 0, \qquad i = 0, 1, 2, 3. \tag{20}$$

The frequencies of vibration ω_i are given by

$$\omega_i^2 = V^0_{ii}/T_{ii}, \tag{21}$$

while for the damping ratios α_i one has

$$\alpha_i = \tfrac{1}{2}R_{ii}/T_{ii}. \tag{22}$$

The potential energy function is independent of q_0, and consequently the frequency of the corresponding mode is zero. The physical reason is that in this mode the system performs only translation and dilation, which have no strain energy within the Donnell approximation.

Let us assume now that the system is static: i.e., $p(t) = p_0 = \text{const}$. Then it is possible to obtain the critical loads for the second and third mode according to the linear buckling theory from the equations

$$V^0_{ii}q_i = W_{ii}q_i, \qquad i = 1, 2, \tag{23}$$

which give a linear system of algebraic equations with unknown p_0. There are no critical loads connected with the first and the last mode in equation (15).

An additional insight into the shell behaviour is provided by the analysis of the total potential energy of the system approximated with a finite number of d.o.f. For a better geometric presentation let us analyze the potential energy function of a system model with two d.o.f. Under static loading the deflection parameters q_1 and q_2 are constant in time in

$$w(x, y) = q_1 h \cos(\pi x/L)\cos(ny/R) + q_2 h \cos(2\pi x/L), \tag{24}$$

and the total potential energy depends on them. We include in this case the contribution of the external static load to the total potential energy. One can apply results from singularity (catastrophe) theory [20] in order to study buckling phenomena [21] systematically. We should point out that a common drawback in the application of catastrophe theory to elasticity problems is the lack of exact expressions for the potential energy. We can easily calculate the necessary results with the aid of computer algebra. In Figure 2 energy contours for $V(q_1, q_2)$ are shown, for the case of $p_0 = 0$. The potential well corresponds to the trivial solution. In Figure 3 energy contours for the case $p_0 \approx \frac{1}{2}p_c$, where p_c is the critical load according to the linear buckling theory, are shown. The system now possesses three potential wells. One of them corresponds to the trivial solution, the other to deformed symmetric in q_1 buckled states. The exact values of q_1 and q_2 at all equilibria are calculated by using the fact that they are critical points of the potential energy function and satisfy the equations

$$\partial V/\partial q_1 = 0, \qquad \partial V/\partial q_2 = 0.$$

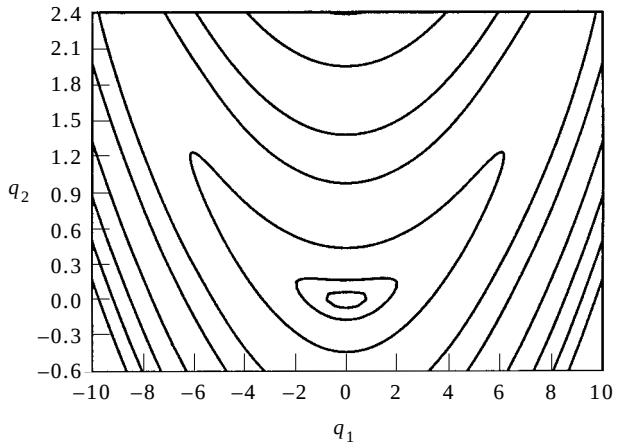

Figure 2. Potential energy contours for a two d.o.f. system; $p_0 = 0$, $h = 0{\cdot}002$ m, $R = 0.2\,m$, $L = 0{\cdot}4$ m, $E = 2{\cdot}1 \times 10^8$ kN/m^2, and $\nu = 0{\cdot}3$.

More exactly at these values of q_1 and q_2, the potential energy has minima. They are zero and $q_1 = \pm 7{\cdot}47320$, $q_2 = 1{\cdot}77566$. There are two other solutions of the above equations which correspond to the saddle points at $q_1 = \pm 4{\cdot}00416$, $q_2 = 0{\cdot}537373$.

Since our main concern in this paper is the parametrically excited vibrations of the shell, it is worth showing the form of the equations in this case. For example, for a system model with two d.o.f. after using an approximation function like equation (24), but with deflection parameters q_1 and q_2 that now depend on the time t, we obtain

$$T_{11}\ddot{q}_1 + R_{11}\dot{q}_1 + (V^0_{11} - W_{11})q_1 + V^0_{112}q_1q_2 + \tfrac{1}{2}V^0_{1122}q_1q_2^2 + \tfrac{1}{6}V^0_{1111}q_1^3 = 0, \tag{25}$$

$$T_{22}\ddot{q}_2 + R_{22}\dot{q}_2 + (V^0_{22} - W_{22})q_2 + \tfrac{1}{2}V^0_{112}q_1^2 + \tfrac{1}{2}V^0_{1122}q_1^2q_2 = 0. \tag{26}$$

In view of the expressions for the different coefficients in the previous section, it is interesting to note that all coefficients are positive except V^0_{112}. The V^0_{112}-terms are responsible for the softening type of structural behaviour observed in a later section.

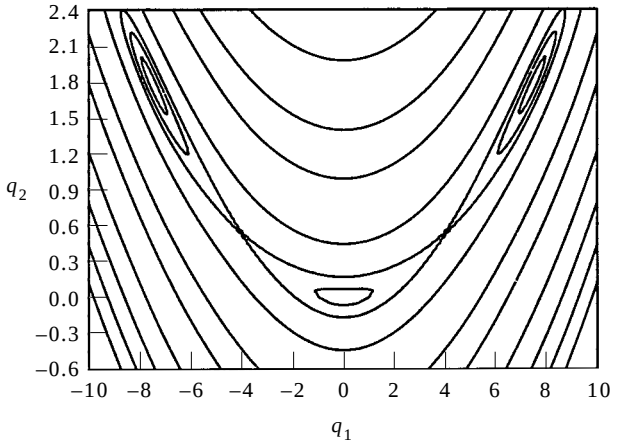

Figure 3. Potential energy contours for a two d.o.f. system, $p_0 \approx \frac{1}{2}p_c$, $h = 0{\cdot}002$ m, $R = 0{\cdot}2$ m, $L = 0{\cdot}4$ m, $E = 2{\cdot}1 \times 10^8$ kN/m^2, and $\nu = 0{\cdot}3$.

In concluding this section we would like to make an additional comment about the approach used. By the use of the Galerkin method one obtains completely the same systems of equations for the problem investigated. At first glance such an approach leads to the necessary equations in a straight manner and with less computational effort. However we should emphasize that our approach is essentially a physical one and it gives an additional insight into the system behaviour through the potential energy function. Concerning the computational issue, the difference is not relevant when using programs for symbolic computations.

6. NUMERICAL CONTINUATION OF SOLUTIONS

In order to analyze dynamical solutions of finite dimensional models in a systematic way, one must apply bifurcation theory. An analytical approach to bifurcations is connected with significant difficulties. Only a few system models have been analyzed completely without the help of numerical methods. Fortunately, there exist numerical continuation techniques (path and bifurcation following methods). With the aid of these methods the analysis is performed within a great precision up to round-off errors. One detects periodic solutions and studies their stability and bifurcations in the parameter space. We will briefly describe the relevant steps involved in the analysis, for more details, see reference [22].

The first step in the numerical continuation of solutions is to determine starting periodic solutions and their stability. The Lagrange equations represent a system of second order ordinary differential equations like equations (25) and (26), which for the numerics is transformed into a system of first order ODEs

$$\dot{z} = f(\mathrm{z}, t, \lambda). \tag{27}$$

Here the vector z contains displacements and velocities while λ contains the system parameters, e.g. the amplitude and/or frequency of excitation. In order that path following methods can be applied and bifurcation diagrams determined, system (27) is transformed into a map. In our case an algebraic system is obtained by calculating Poincaré stroboscopic maps [23, 24].

System (27) is integrated over time intervals which are multiples of the period of excitation. In this way the periodic solutions correspond to the fixed points of the algebraic equations

$$F(z, \lambda) = P^k(z, \lambda) - z = 0. \tag{28}$$

In equation (28) z denotes a k-periodic solution (with period k-times the period of the external excitation), and $P^k(z, \lambda)$ is a Poincaré map obtained by numerical integration. The Jacobian matrix of map F

$$D_z F(z, \lambda) = D_z P^k(z, \lambda) - I \tag{29}$$

is also necessary for our routines. In equation (29) I is the identity matrix. The $D_z P^k(z, \lambda)$-matrix is governed by the first variational equation of the original system for the monodromy matrix ψ,

$$\dot{\psi} = D_z f(z, t, \lambda)\psi, \tag{30}$$

with initial conditions

$$\psi(0) = I, \tag{31}$$

and is obtained again by integrating over time intervals which are multiples of the period of excitation.

Stability of solutions is examined by using equation (29). If all eigenvalues of $D_z P^k(z, \lambda)$ lie in the unit circle the motion is stable, otherwise unstable. Period doubling bifurcations are indicated by an eigenvalue that crosses the unit circle at -1. Pitchfork, transcritical bifurcations and saddle-node folds are indicated by an eigenvalue that crosses the unit circle at $+1$ [24].

When one is interested only in the dependence of the solutions on one parameter ($\lambda \in \mathbf{R}$) the problem has the following formulation [22]; find a one-parameter family of solutions of the under-determined system

$$F(y) = 0 \qquad \text{with} \qquad F\colon \mathbf{R}^{n+1} \mapsto \mathbf{R}^n, \tag{32}$$

where $y = (z, \lambda)$.

The complete continuation procedure keeps track of the whole path of periodic solutions and looks for bifurcation points, where branches of different periodic solutions intersect. In order to compute subsequent points on a branch we use the tangent of the path given by the Jacobian matrix of the Poincaré map with respect to the control parameter. The continuation of solutions is performed with the help of predictor-corrector steps. Predictor:

$$y_1^* = y_0 + s\Delta y \qquad \text{with tangent vector} \qquad \Delta y = \text{null}\,(DF(y_0)), \tag{33}$$

where s is a suitably chosen continuation step. Corrector with successive (Newton) iterations:

$$y_1^{k+1} = y_1^k - DF(y_1^k)^+ F(y_1^k), \quad k = 1, 2, \ldots \qquad \text{where} \qquad y_1^0 = y_1^*, \tag{34}$$

and DF^+ is the Moore–Penrose pseudo-inverse matrix. The efficiency of the continuation strongly depends on the proper choice of the step size s [22].

A special procedure is needed for singular points: i.e., when $\text{rank}(DF(y)) < n$. By examining carefully those points we know exactly what types of bifurcations occur in the original vibration problem.

The most expensive part of the numerical continuation of solutions is the numerical integration of the system of ODEs, which is performed by appropriate numerical schemes. We use specifically DOP853 of reference [25] which is an explicit Runge–Kutta integrator.

7. ANALYSIS OF THE RESULTS

By using continuation techniques a bifurcation analysis is performed for system equations similar to equations (25) and (26), and obtained by the Langrange method.

In order to deal with physically relevant parameters, let us take $h = 0{\cdot}002$ m, $R = 0{\cdot}2$ m, $L = 0{\cdot}4$ m for the shell geometry: i.e., $R/h = 100$ and $L/R = 2$. The material properties correspond to steel with $E = 2{\cdot}1 \times 10^8$ kN/m^2, $\nu = 0{\cdot}3$ and $m = 15{\cdot}7$ kg/m^2. Air damping with coefficient $\beta_1 = 1{\cdot}59$ kNs/m is adopted which is 1·6% of the critical damping in the linear case at the lowest mode that we will consider. The material damping is $\beta_2 = \eta D$, where $\eta = 0{\cdot}0001$ is appropriate for steel. For these values of the key parameters, bifurcation diagrams are calculated for varying amplitude p_1 and frequency of excitation ω. It is more convenient to use the non-dimensional parameter $\mu = p_1/2(p_c - p_0)$ instead of p_1 as an excitation parameter, where p_c is the critical load according to the linear buckling theory. For example when $\mu = 0{\cdot}5$ then the loading reaches the critical load p_c only instantly, while e.g., for $\mu = 0{\cdot}75$ it spends a significant amount of time with values greater than the critical one; see Figure 4.

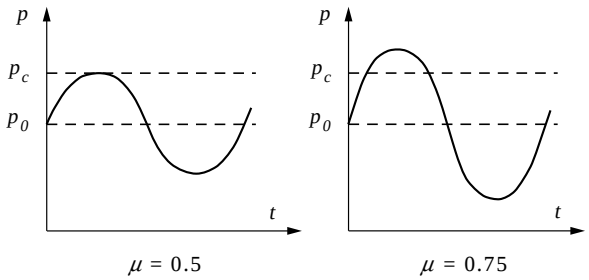

Figure 4. Dynamical load for two different values of μ.

We will discuss bifurcation diagrams for models which involve only two of the lowest modes of vibrations

$$f_1(t)h \cos(\pi x/L) \cos(5y/R), \qquad \text{mode 1},$$

$$f_2(t)h \cos(\pi x/L) \cos(6y/R), \qquad \text{mode 2},$$

in conjunction with

$$f_3(t)h \cos(2\pi x/L), \qquad \text{mode 3}.$$

It is worth pointing out that in our preliminary unpublished studies we included "rosette" modes like

$$q_3(t)h \cos(2ny/R), \qquad \text{waves only in the circumferential direction},$$

in the analysis, but our results suggested that they are without relevance. In other words, they do not cause any qualitative changes at the bifurcation diagrams discussed.

By taking different values for the frequency of excitation ω, different modes can be excited. This is an important point to remember when comparing results for statically and dynamically loaded shells. The number of important modes is much more limited when studying elastic stability. In our case we take such values for the frequency of excitation ω that the above mentioned modes are of importance; i.e., they are excited by the loading.

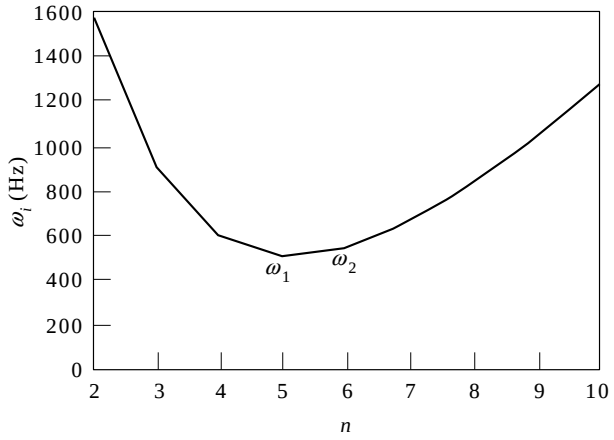

Figure 5. Frequency versus number of waves in the circumferential direction.

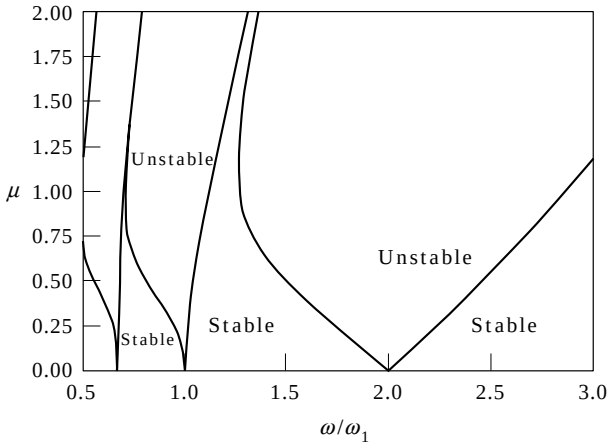

Figure 6. Ince–Strutt diagram for the linear system.

7.1. THE CASE $p_0 = 0$

Let us assume for now that the constant part of the loading p_0 is equal to zero. By linear analysis the circular frequency of mode 1 is $\omega_1 = 503{\cdot}7$ Hz, of mode 2 $\omega_2 = 547$ Hz, while that of mode 3 is $\omega_3 = 4117$ Hz. The ratio between the first two frequencies, $\omega_2/\omega_1 = 1{\cdot}086$, indicates a condition close to an internal resonance. One can see the dependence of the frequency on the number of waves in the circumferential direction in Figure 5.

We study bifurcations of the trivial solution, namely the transition from purely extensional to bending oscillations. We are looking for significant changes in the bifurcation diagrams caused by the inclusion of different modes.

A good starting point for the analysis is probably to recall some well-known facts from dynamical stability theory [8]. The ordinary differential equation which describes the motion at mode 1 is of the form (25). After linearizing, neglecting the damping and re-scaling it is possible to bring the equation into the form of a classic Mathieu equation

$$\frac{\mathrm{d}^2 f_1}{\mathrm{d}\tau^2} + \left[1 - 2\mu \cos\left(\frac{\omega}{\omega_1}\tau\right)\right] f_1 = 0, \tag{35}$$

where τ is a new non-dimensional time variable. This equation can be solved in terms of Mathieu functions [26]. The stability of the trivial (zero) solution is completely determined by making use of the so-called Ince–Strutt diagram, Figure 6, which is obtained here with exact Mathieu functions from reference [26]. The linear analysis says that in the zones of instabilities the amplitudes of the solutions grow exponentially, which is not the case when non-linearities come into play. The zone which starts at $\omega/\omega_1 = 2{\cdot}0$ is usually known as the principal parametric resonance, while that one at $\omega/\omega_1 = 1{\cdot}0$ is the fundamental parametric resonance, respectively.

We begin the non-linear analysis with mode 1 only. Our methods make it possible to understand completely how the trivial solution loses its stability. As suggested by the linear analysis, the interesting phenomena occur in the zones of the parametric and fundamental resonances. There are several possible ways for the loss of stability of the trivial solution. The transition in the area of the principal parametric resonance is through an eigenvalue equal to -1 (see Figure 7), while in the area of the fundamental resonance it is through an eigenvalue equal to $+1$. In the first case we have period doubling bifurcations, while in the second one the transition is to other solutions with period equal to the period of

excitation. A more detailed analysis reveals in the first case possible super- (line S_p^1) and sub-critical (line S_b^1) flip bifurcations while in the second case pitchfork bifurcations (lines S_p^2 and S_b^2) occur (see Figures 8–12). In all figures which follow the numerical value at the upper right corner stands for ω/ω_1. A dotted line means unstable solutions, and the displacement is for a value at a Poincaré section of the periodic solution investigated. The periodicity of the solutions is also shown by values which are multiples of the period of the external excitation $T = 2\pi/\omega$. The parameter range in Figures 8–12 is indicated by lines F8–F12 in Figure 7. Lines B^1 and B^2 denote saddle-node folds. A more complicated picture is shown in Figure 10 where our cross-section "hits" three bifurcation lines. Not all possible bifurcations are shown in Figure 7 for reasons of clarity, for a more detailed picture of a simpler problem see references [27, 28].

The shell behaviour obtained by the first mode corresponds to a hardening type of oscillation: i.e., the amplitude of vibration increases with the increase of the frequency of parametric excitation. This type of behaviour is observed qualitatively by analyzing other single "linear" modes, and in particular mode 2. The behaviour changes completely by the inclusion of mode 3 into the analysis. Now the system shows a softening type of behaviour; see Figure 13, and Figures 14–18. One can easily see that the system behaviour reverses its type; e.g., compare Figure 7 with Figure 13.

This last type of behaviour is in a better agreement with the experimental results [6]. We shall note that this result presents a genuine mode interaction. The change of behaviour is due only to the coupling between modes 1 and 3. On the other hand there are no changes at the exact value of the occurrence of the first bifurcation in the trivial solution, which is not surprising as these values can be obtained even by means of linear stability analysis (see Figure 6). The other important feature of the motion is that in the zone of the principal resonance the change is manifested by jumps to solutions with much higher amplitudes.

The next interesting set of results corresponds to $\omega/\omega_1 = 2{\cdot}4$, and $\omega/\omega_2 = 2{\cdot}21$, thus, closer to the principal resonance in mode 2. Taken on their own both modes show the typical behaviour for this parameter range; see Figures 19–20, and compare them with Figure 8. Though taken together both "linear" modes interact with each other; and the loss of stability occurs firstly at mode 2. The displacements and velocities at mode 1 are zero for all bifurcation branches shown in Figure 21, although by comparison with Figure 20 one sees the change of stability due to the presence of mode 1. The inclusion of mode 3 changes the behaviour completely, as one can see in Figure 22 very short stable branches.

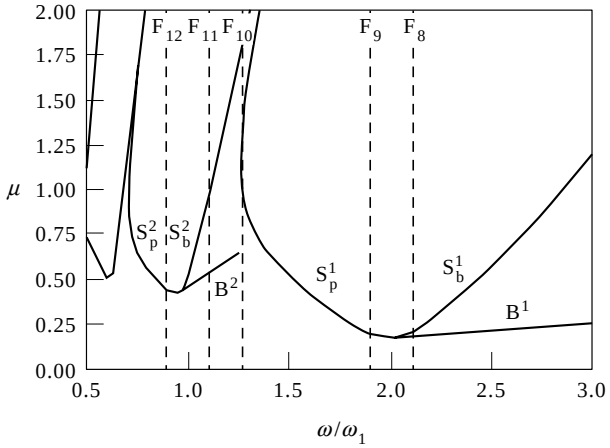

Figure 7. Stability change types: mode 1.

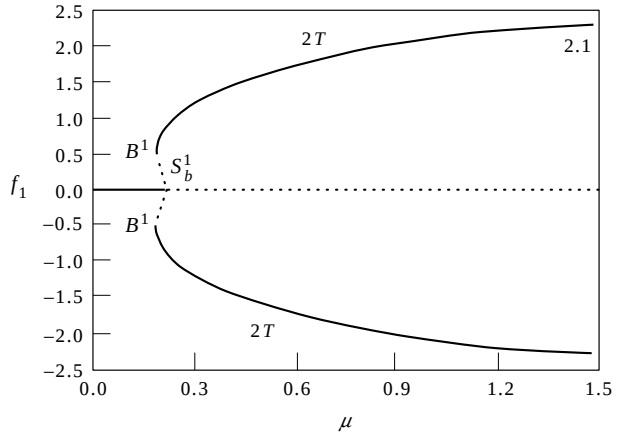

Figure 8. Subcritical flip bifurcation, $p_0 = 0$: mode 1.

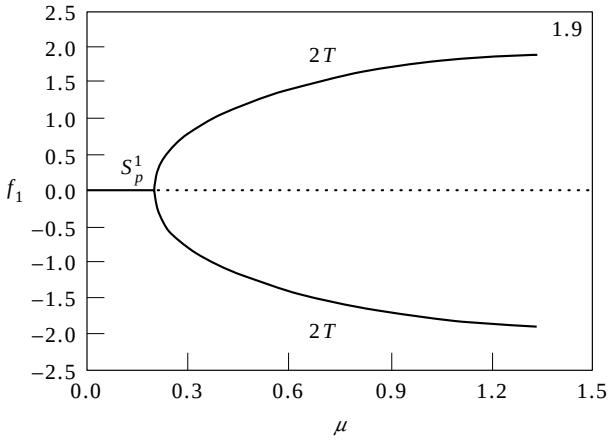

Figure 9. Supercritical flip bifurcation, $p_0 = 0$: mode 1.

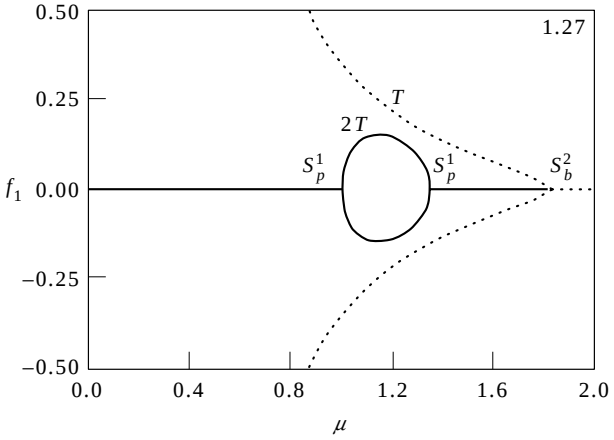

Figure 10. A more complicated behaviour, $p_0 = 0$: mode 1.

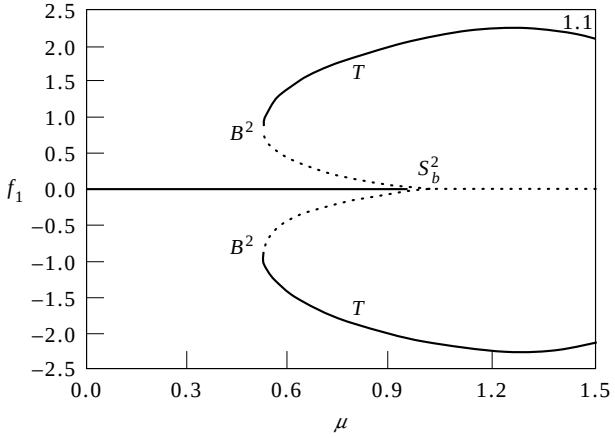

Figure 11. Subcritical pitchfork bifurcation, $p_0 = 0$: mode 1.

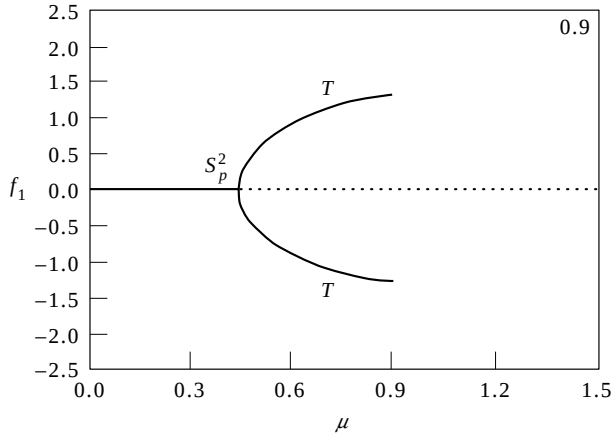

Figure 12. Supercritical pitchfork bifurcation, $p_0 = 0$: mode 1.

The next bifurcation of the trivial solution occurs at mode 1 (Figure 23), and it is without physical relevance despite the fact that the solution stabilizes at a greater excitation level. The parameter value of the bifurcation in mode 2 is also indicated in Figure 23.

7.2. THE CASE $p_0 \approx \frac{1}{2} p_c$

Let us assume that the constant part of the loading $p_0 = 1275$ kN/m, which is almost half the critical load according to the linear buckling theory. Now by linear analysis the frequency of mode 1 is $\omega_1 = 356{\cdot}2$ Hz, of mode 2 $\omega_2 = 415{\cdot}2$ Hz, while that of mode 3 is $\omega_3 = 4056$ Hz. The ratio between the first two frequencies is $\omega_2/\omega_1 = 1{\cdot}166$.

We performed essentially an analysis analogous to that for the case $p_0 = 0$ and obtained qualitatively the same results. The differences are mainly in the values of the occurrence of the bifurcations. The other peculiarity is that we study stability not only of the trivial solution but of those solutions which correspond to the deformed states (Figure 3), not available in the previous case with $p_0 = 0$.

In Figures 24 and 25, we show the transition from hardening to softening type of behaviour with the inclusion of mode 3. These figures may be compared with Figures 8

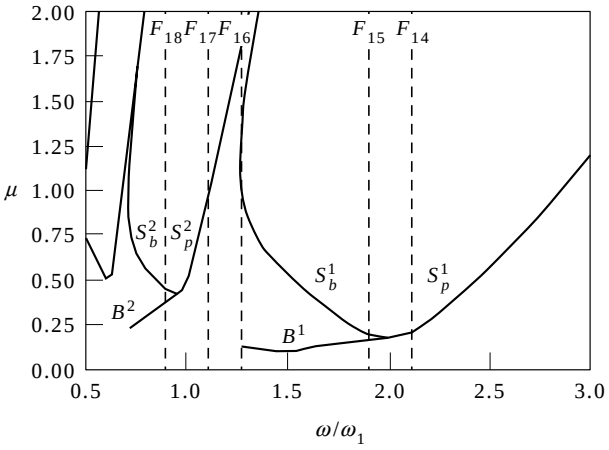

Figure 13. Stability change types: modes 1 + 3.

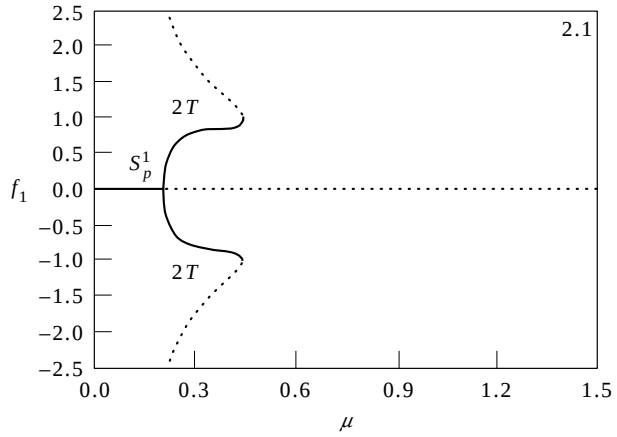

Figure 14. Supercritical flip bifurcation, $p_0 = 0$: modes 1 + 3.

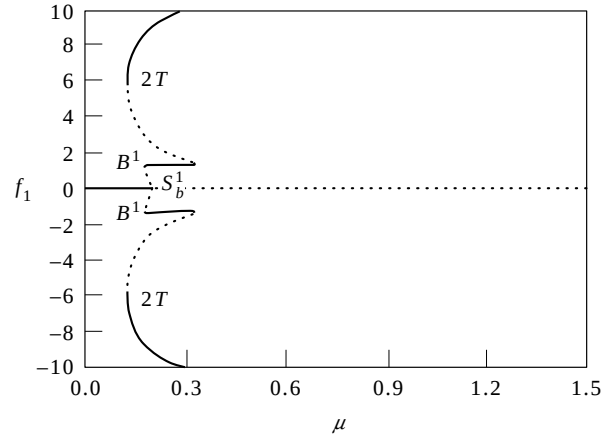

Figure 15. Subcritical flip bifurcation, $p_0 = 0$: modes 1 + 3.

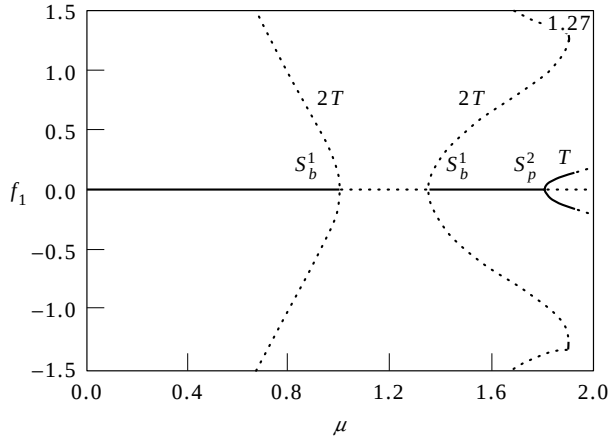

Figure 16. A more complicated behaviour, $p_0 = 0$: modes 1 + 3.

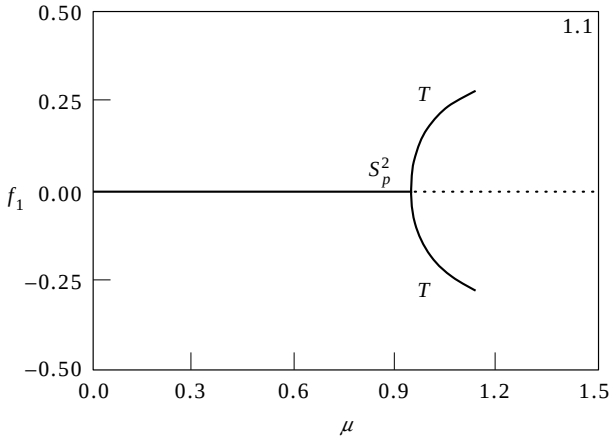

Figure 17. Supercritical pitchfork bifurcation, $p_0 = 0$: modes 1 + 3.

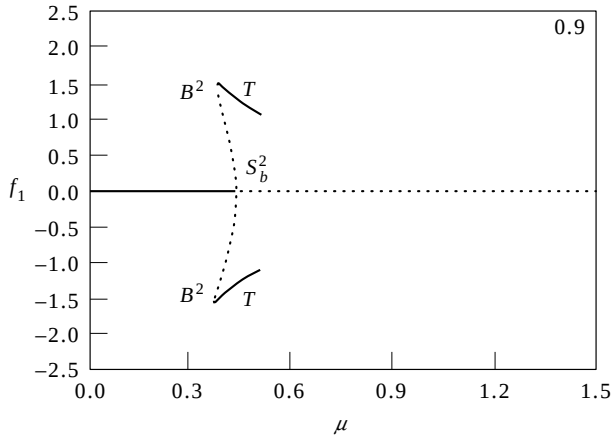

Figure 18. Subcritical pitchfork bifurcation, $p_0 = 0$: modes 1 + 3.

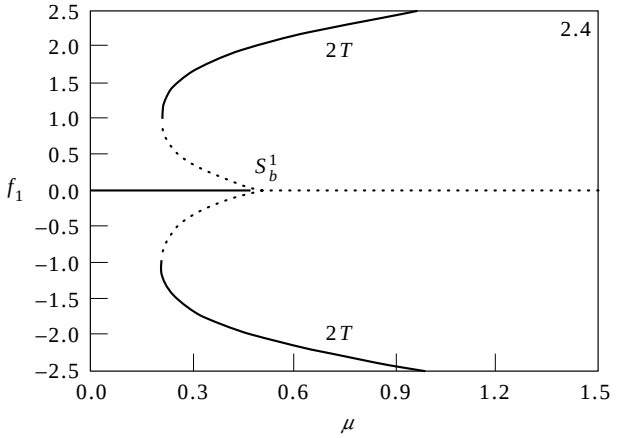

Figure 19. Subcritical flip bifurcation, $p_0 = 0$: mode 1.

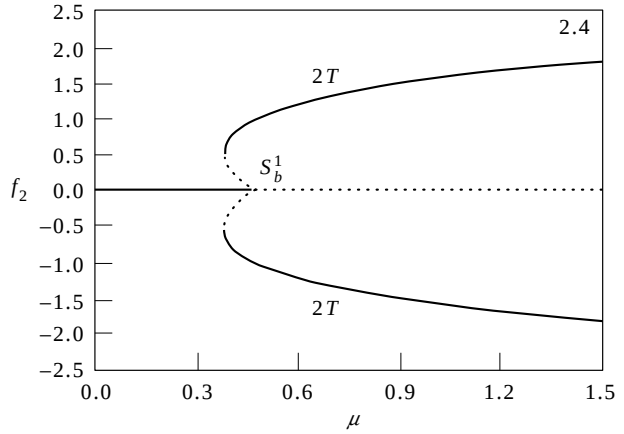

Figure 20. Subcritical flip bifurcation, $p_0 = 0$: mode 2.

and 14. We do not include other figures because we obtained qualitatively the same results as those shown in Figures 7–18 with differences only in the exact values.

The interaction between modes 1, 2 and 3 is illustrated in Figures 26 and 27 (see Figures 22 and 23, respectively). Besides the different displacement and velocity values, there is a change at the first bifurcation of the trivial solution, which now occurs at mode 1 first.

A more complete bifurcation analysis in this case reveals other solution branches (see Figures 28 and 29). The solution in Figure 28 corresponds to parametric oscillations in the vicinity of a "deformed" shell equilibrium, after buckling snap-through. The notation PD stands for period doubling bifurcations, while SN for a saddle-node bifurcation. The important point is that at $\mu = 0{\cdot}0$, the stable and unstable part of this solution branch start at values for the displacement equal to $f_1 = 7{\cdot}47320$ and $f_1 = 4{\cdot}00416$, respectively, which correspond precisely to one of the "deformed" equilibrium and a saddle point in the potential energy function. When the amplitude of excitation reaches the upper critical load p_c both solutions disappear in a saddle-node bifurcation: point SN in Figure 28. There is one other solution branch which corresponds to the other potential well in Figure 3, with the same but negative values of the displacements.

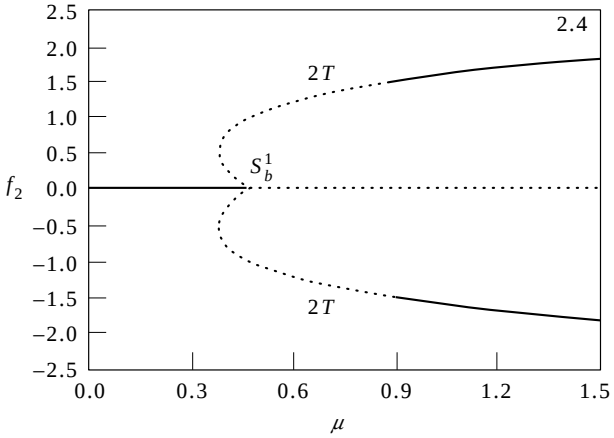

Figure 21. Mode interaction, $p_0 = 0$: modes $1 + 2$.

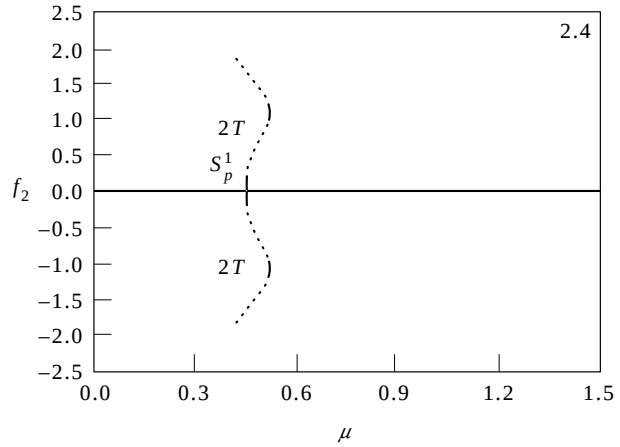

Figure 22. Mode interaction, $p_0 = 0$: modes $1 + 2 + 3$.

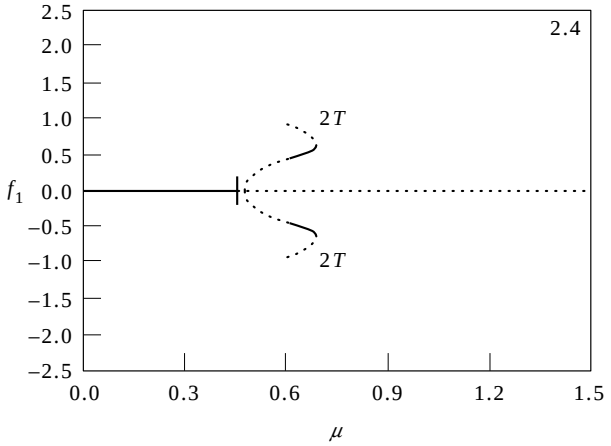

Figure 23. Mode interaction, $p_0 = 0$: modes $1 + 2 + 3$.

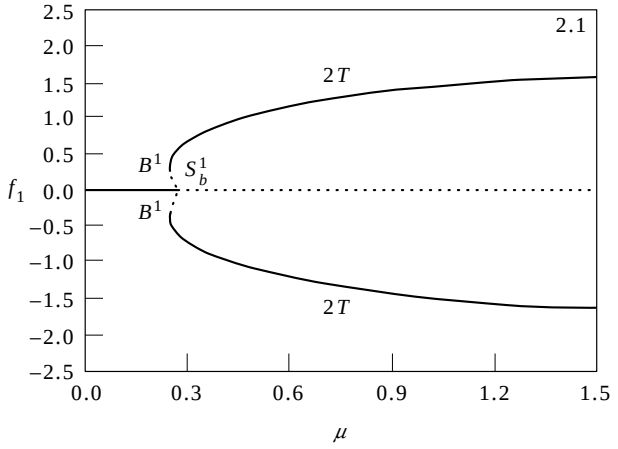

Figure 24. Subcritical flip bifurcation, $p_0 \approx \frac{1}{2}p_c$: mode 1.

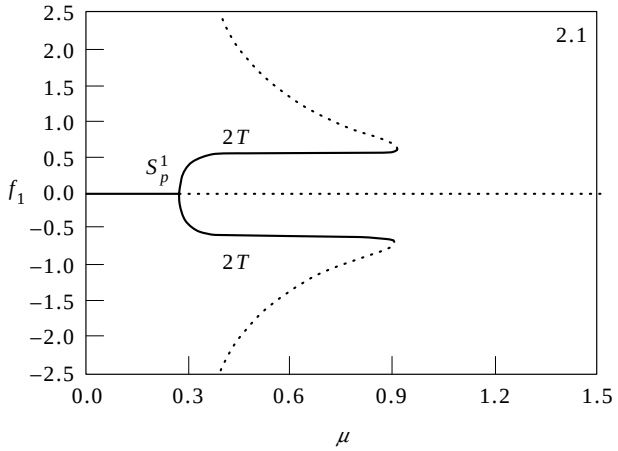

Figure 25. Supercritical flip bifurcation, $p_0 \approx \frac{1}{2}p_c$: modes $1 + 3$.

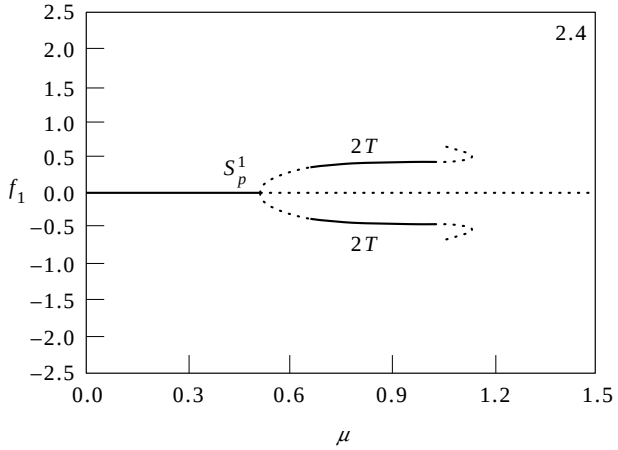

Figure 26. Mode interaction, $p_0 \approx \frac{1}{2}p_c$: modes $1 + 2 + 3$.

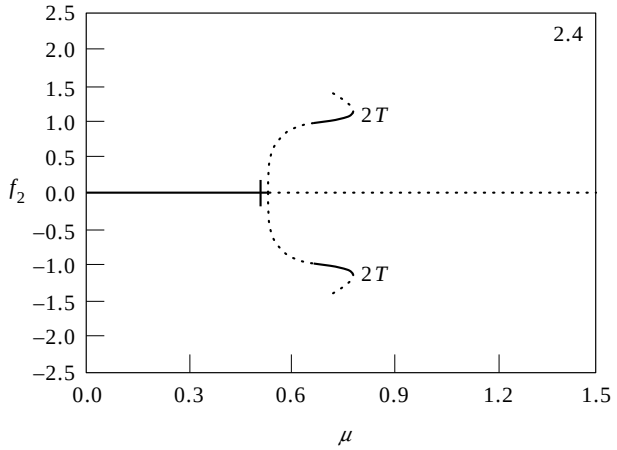

Figure 27. Mode interaction, $p_0 \approx \frac{1}{2} p_c$: modes $1 + 2 + 3$.

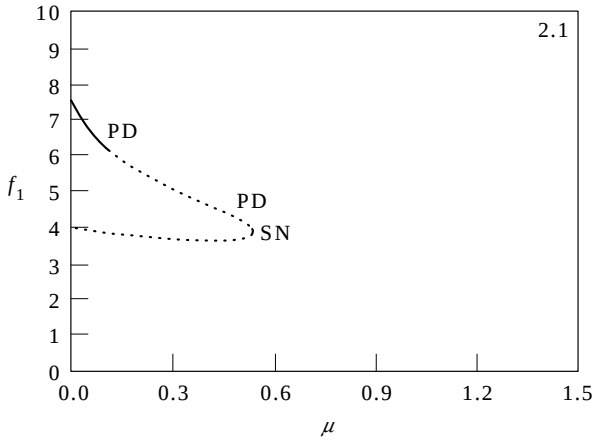

Figure 28. Bifurcation of the buckled state solution, $p_0 \approx \frac{1}{2} p_c$: modes $1 + 3$.

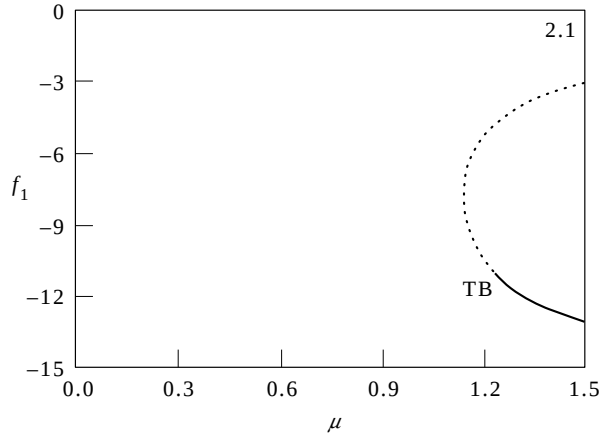

Figure 29. Another solution, $p_0 \approx \frac{1}{2} p_c$: modes $1 + 3$.

Finally, we would like to point out that there are other solutions with amplitudes greater than those discussed above, which are more global in nature like those shown in Figure 29, where TB means transcritical bifurcation.

8. CONCLUDING REMARKS

In our opinion, with the introduction and the wide use of finite element packages the interesting fundamental problems of shell behaviour have been widely ignored. The main area of scientific research seems to focus on numerical methods, their implementations, and composite structures. Despite the fact that such approaches are very useful for practical structural design, we are in doubt about their utility towards the understanding of shell dynamics. A finite element model of a typical engineering system usually has around 100 elements. Thus, the infinite dimensional continuum is approximated by a phase space of order 10^2 to 10^3. This is still far too great to facilitate standard dynamical systems techniques such as continuation methods.

In this paper we have demonstrated how a suitable combination of analytical and numerical computer methods can be used for the analysis of modal interactions in shell structures. Our approach makes it possible to reveal fine details in the bifurcation diagrams and to calculate with great precision all bifurcation points. On the other hand we are able to show that with appropriate approximation functions, results in good agreement with experiments can be obtained. With the inclusion of suitable modes of vibration, the cylindrical shell shows a softening type of behaviour, characteristic of real experiments [6]. We obtained qualitatively the same sort of results for two different values of the constant part of the loading p_0 which contradicted our preliminary expectations.

ACKNOWLEDGMENT

The research of AAP was supported by a research grant from the Engineering and Physical Sciences Research Council (EPSRC) of the UK under the Applied Nonlinear Mathematics Initiative.

REFERENCES

1. C. R. Calladine 1983 *Theory of Shell Structures*. Cambridge: Cambridge University Press.
2. L. H. Donnell 1976 *Beams, Plates, and Shells*. New York: McGraw-Hill.
3. S. P. Timoshenko and J. M. Gere 1961 *Theory of Elastic Stability*. New York: McGraw-Hill.
4. S. P. Timoshenko and S. Woinowsky-Krieger 1959 *Theory of Plates and Shells*. New York: McGraw-Hill.
5. A. S. Wolmir 1962 *Biegsame Platten und Schalen*. Berlin: Verlag für Bauwesen.
6. D. A. Evensen 1974 In *Thin-Shell Structures* (Y. C. Fung and E. E. Sechler, editors). Englewood Cliffs, NJ: Prentice-Hall. Nonlinear vibrations of circular cylindrical shells.
7. A. S. Volmir 1972 *Nonlinear Dynamics of Plates and Shells*. Moscow: Nauka (in Russian).
8. V. V. Bolotin 1964 *The Dynamic Stability of Elastic Systems*. San Francisco: Holden-Day.
9. C. S. Hsu 1974 In *Thin-Shell Structures* (Y. C. Fung and E. E. Sechler, editors). Englewood Cliffs, NJ: Prentice-Hall. On parametric excitation and snap-through stability problems of shells.
10. J. C. Yao 1963 *AIAA Journal* **1**, 1391–1396. Dynamic stability of cylindrical shells under static and periodic axial and radial loads.
11. R. S. Roth and J. M. Klosner 1964 *AIAA Journal* **2**, 1788–1794. Nonlinear response of cylindrical shells to dynamic axial loads.
12. J. C. Yao 1965 *Journal of Applied Mechanics* **32**, 109–115. Nonlinear elastic buckling and parametric excitation of a cylinder under axial loads.
13. A. H. Nayfeh and B. Balachandran 1989 *Applied Mechanics Reviews* **42**(11), Part 2, S175–S201. Modal interactions in dynamical and structural systems.

14. J. M. T. Thompson and J. R. de Souza 1996 *Proceedings of the Royal Society of London* **A452**, 2527–2550. Suppression of escape by resonant modal interactions: in shell vibration and heave-roll capsize.
15. Y. C. Fung, E. E. Sechler and A. Kaplan 1957 *Journal of The Aeronautical Sciences* **24**, 650–660. On the vibration of thin cylindrical shells under internal pressure.
16. V. D. Kubenko, P. S. Kovalchuk and T. S. Krasnopolskaya 1984 *Nonlinear Mode Interaction of Bending Vibrations in Cylindrical Shells*. Kiev: Naukova Dumka (in Russian).
17. E. H. Dowell and C. S. Ventres 1968 *International Journal of Solids and Structures* **4**, 975–991. Modal equations for the nonlinear flexural vibrations of a cylindrical shell.
18. G. W. Hunt, K. A. J. Williams and R. G. Cowell 1986 *International Journal of Solids and Structures* **22**, 1501–1515. Hidden symmetry concepts in the elastic buckling of axially-loaded cylinders.
19. H. Goldstein 1980 *Classical Mechanics*. Reading, MA: Addison-Wesley.
20. T. Poston and I. Stewart 1978 *Catastrophe Theory and its Application*. London: Pitman.
21. J. M. T. Thompson and G. W. Hunt 1984 *Elastic Instability Phenomena*. Chichester: Wiley.
22. E. Allgower and K. Georg 1990 *Numerical Continuation Methods*. Berlin: Springer-Verlag.
23. J. Guckenheimer and P. Holmes 1983 *Nonlinear Oscillations*, *Dynamical Systems*, *and Bifurcations of Vector Fields*. Berlin: Springer-Verlag.
24. J. M. T. Thompson and H. B. Stewart 1986 *Nonlinear Dynamics and Chaos*. Chichester: Wiley.
25. E. Hairer, S. Nørsett and G. Wanner 1993 *Solving Ordinary Differential Equations*. *I*. *Nonstiff Problems* (second revised edition). Berlin: Springer-Verlag.
26. N. W. McLachlan 1947 *Theory and Application of Mathieu Functions*. Oxford: Clarendon Press.
27. M. S. Soliman and J. M. T. Thompson 1992a *Proceedings of the Royal Society of London* **A438**, 511–518. Indeterminate sub-critical bifurcations in parametric resonance.
28. M. S. Soliman and J. M. T. Thompson 1992b *Proceedings of the Royal Society of London* **A439**, 601–610. Indeterminate trans-critical bifurcations in parametrically excited systems.